Calculation of the Raman Spectrum of Photodissociating H_2S around 195 nm†

Dimitris Skouteris, Bernd Hartke, and Hans-Joachim Werner*

Institut für Theoretische Chemie, Universität Stuttgart, Pfaffenwaldring 55, D-70569 Stuttgart, Germany

Received: October 5, 2000; In Final Form: January 11, 2001

Calculated Raman spectra of photodissociating H_2S in its first absorption band are presented, obtained by time dependent wave packet propagation on two coupled diabatic excited-state surfaces, a bound one (of B_1 symmetry in C_{2v}) and a repulsive one (A_2 symmetry). Both of these states are of A″ symmetry in the C_s group and have a conical intersection in the Franck−Condon region. Predicted Raman spectra are presented for four excitation wavelengths in the range of 185−205 nm, and various features of the spectra are explored and compared with experimental data. The different behavior of [*n*00] lines (those involving vibrational excitation in one H−S bond only, in the local mode picture) to that of other [*n*10] and [*nm*1] lines (involving one stretching quantum in one H−S bond and one bending quantum, respectively) is explained using the cross-correlation functions of the propagating wave packet with ground-state wave functions.

1. Introduction

The study of photodissociation of small molecules is an ideal tool for the elucidation of both long- and short-time dynamics on their potential energy surfaces. In the past decade, both experimental and theoretical advances in this field, especially the improvement of the quality of ab initio potential energy surfaces, have made possible the direct comparison between calculations and measurements. The information that can be obtained from the study of photodissociation is of a diverse nature, depending on the actual kind of experiment performed. One kind is pure absorption spectroscopy, whereby the absorption cross section of the dissociating molecule in the region of the photodissociation band is measured as a function of the excitation wavelength. These experiments give information primarily on the dynamics around the Franck−Condon (FC) region, with the overall width of the band indicating the lifetime of the excited state in accordance with the energy−lifetime uncertainty principle. Such experiments have been performed on both H_2S and D_2S by Lee et al.[1] in the first absorption band and theoretically studied by Schinke and co-workers.[2−5] On the other hand, study of the photodissociation products, and in particular the partial photodissociation cross sections pertaining to given product internal states, yields information about the entire region of the exit channel and therefore its theoretical simulation presents a much greater challenge as far as theoretical calculations are concerned. Both vibrational[6−8] and rotational[9−11] distributions of the H−S photofragments have been observed experimentally and predicted theoretically.[4,12,13] These two methods are now well-established tools for studying molecular photodissociation.

A third kind of experimental study is that of the emission spectra of photodissociating molecules. This is essentially the study of a resonance Raman process, the absorption of one photon promoting the molecule to the excited state, followed by return of the molecule to the ground state via the emission of a photon of higher wavelength during the course of the photodissociation. The probability of this effect is generally very small (especially for fast, direct photodissociation), and this makes its experimental detection particularly difficult. However, such experimental data can give information about the dynamics *between* the FC region and the exit channel, i.e., in a way complementary to both of the methods described previously. Since this is a *resonance* Raman process rather than a regular one, i.e., the excitation wavelength matches the energy difference between two electronic states, the Raman spectrum will in general not be purely *static*. In other words, it will not be determined solely by the nuclear coordinate dependence of the transition dipole, but also *dynamic* effects will play a significant role, according to the definition given by Lee and Heller.[14] As has been noted earlier by one of the authors,[15] these effects constitute a stringent test of the accuracy of the potential energy surfaces and nonadiabatic couplings.

In the case of H_2S, there has been a lot of theoretical effort in trying to elucidate the structure of the excited-state potential energy surfaces and the precise nature of the dynamics occurring on them.[2−5,12,13,16,17] A significant amount of controversy has resulted, regarding the question of the "boundedness" or "repulsiveness" of each of the surfaces involved as well as their respective symmetry species. For instance, it has been suggested that the photodissociation dynamics of H_2S is best explained through a model that involves initial promotion of the molecule to a repulsive state, which interacts with a bound one through a bound-continuum Fano mechanism.[12] The opposite model (promotion to a bound state and interaction with a repulsive one) has also been proposed.[6] The most recent ab initio calculations (see below) and dynamical simulations of the absorption spectrum,[2,3,13] and the partial photodissociation cross sections on these surfaces have shown unambiguously that the latter model is the correct one.

Ab initio potential energy surfaces for the excited states under consideration have been calculated previously by Shih et al.,[18] Weide et al.,[19] Theodorakopoulos et al.,[20] Heumann et al.,[2] and more recently, in our group by Simah et al.[13] All calculations show that two surfaces are directly involved in the process. One is of B_1 symmetry in the C_{2v} point group and is of a bound nature, whereas the other is repulsive and of A_2 symmetry. Both

† Part of the special issue "Aron Kuppermann Festschrift".

* Corresponding author. E-mail address: werner@theochem.uni-stuttgart.de.

10.1021/jp0036691 CCC: $20.00
Published on Web 02/17/2001

surfaces are of A″ symmetry in the C_s point group and are hence subject to nonadiabatic coupling. In fact, as already found by Heumann et al.,[2,19] for a fixed bond angle there are two conical intersections on the C_{2v} line quite close to the FC region, and therefore the nonadiabatic coupling plays a crucial role for the dissociation dynamics. The excitation from the ground-state surface (A_1 in C_{2v}) initially occurs primarily to the bound (B_1) surface because of electric dipole selection rules. H_2S subsequently predissociates through nonadiabatic coupling to the repulsive (A_2) surface. Initial motion along the symmetric stretch coordinate on the bound surface produces structure in the UV/VIS absorption spectrum of H_2S (which was initially thought to be due to the bending motion[6,21]). The nonadiabatic effects make the dissociation dynamics of H_2S radically different from that of H_2O. In the latter case[22,23] there is only one repulsive surface involved in the excited state (of B_1 symmetry in the C_{2v} point group), and the Born−Oppenheimer approximation can be safely employed.

Calculations on the Raman emission of photodissociating H_2S have already been performed by Heumann and Schinke[5] using the time dependent wave packet method, and many of the features of the predicted spectra were discussed and elucidated. In particular, a qualitatively different behavior of the cross-correlation functions and the wavelength dependence of the cross sections for the $[n0^+0]$ and $[(n-1)1^+0]$ final states was found, where $[mn^+k]$ denote excitations with m, n quanta in the two local SH stretching modes, respectively, and k quanta in the bending mode. However, despite the fact that the calculated absorption spectra as well as partial photodissociation cross sections were in reasonably good agreement with experimental results, the agreement of the computed Raman spectra with existing experimental data of Brudzynski et al.[24] was less satisfactory. The authors concluded that more accurate ab initio calculations and diabatization procedures were desirable in order to obtain a better understanding of the experimental observations.

As mentioned before, the two relevant adiabatic excited-state surfaces have conical intersections near the FC region, leading to very strong nonadiabatic couplings. The dynamics calculations are most conveniently performed in a quasi-diabatic representation, in which the electronic wave functions are smoothly varying as function of geometry and the derivative couplings are assumed to be zero. Instead, a diabatic coupling potential occurs. The diabatization transformation is nonunique, and various approximate diabatization schemes have been used before for H_2S.[4,5,13] In the original work by Heumann et al.[4] the adiabatic mixing angle was determined from the condition that the CI vectors of the excited-state electronic wave functions should vary as little as possible relative to reference geometries in C_{2v} symmetry (in which diabatic and adiabatic wave functions are identical by definition). This method did not take into account a possible change of the orbitals as function of geometry, and therefore eliminated the derivative couplings only partly. Consequently, the diabatic coupling potential was too weak, leading to too narrow bands in the absorption spectrum. In later work, Heumann and Schinke[5] proposed an alternative method, in which the nonadiabatic mixing was determined from the condition that the transition dipole moments between the ground state (A_1) and the repulsive (A_2) diabatic state should vanish at all geometries. They found that this improves the width of the absorption spectrum and in particular the Raman spectrum. However, the condition that one of the transition dipole moments vanishes in C_s symmetry is not strictly valid. Therefore, also in this case the derivative couplings are not entirely eliminated, and again the coupling in the diabatic basis is too weak. In the most recent calculations by Simah et al.,[13] the diabatization condition was that both the orbitals as well as the CI vectors of the electronic wave functions change as little as possible relative to reference geometries in C_{2v} symmetry. This fully minimizes the derivative coupling matrix elements and leads to an almost quantitative agreement of the computed and experimental absorption spectra.

The purpose of the present work is to investigate if the new surfaces and the improved diabatization scheme of Simah et al.[13] lead to better agreement of the calculated and experimental Raman emission spectra, and furthermore to explore in more detail the reason for the previous and remaining discrepancies. For comparison, we have also applied the diabatization method of Heumann et al. using transition dipole moments to demonstrate the effect of the diabatization scheme on the dynamics. As already pointed out by Heumann and Schinke,[5] the Raman emission spectra are very sensitive to the nonadiabatic coupling and therefore the H_2S molecule presents a particular challenge for this kind of theoretical study.

In section 2, a brief overview of the time-dependent theory of Raman scattering is presented. In section 3 the details of the method used are given, and the results are discussed and compared with experimental data in section 4. Finally, a conclusion is presented in section 5.

2. Theory

The time-dependent theory of Raman scattering has been analyzed thoroughly by Lee and Heller[14] as well as Loudon,[25] Schinke,[26] and Hartke,[27] and compared with the corresponding time-independent theory which leads to the well-known Kramers−Heisenberg−Dirac expression.[28,29] Within the time-dependent approach, the initial wave packet is the product of the ground-state nuclear wave function and the transition dipole moment function. Since in this case there are two excited state surfaces involved, the wave packet is expressed as a two-component vector. This function is subsequently propagated on the two excited-state surfaces, according to the time-dependent Schrödinger equation. At each point in the propagation, a cross-correlation function is calculated for each of the ground state vibrational levels that is of interest (i.e., to which the excited state is likely to decay through Raman emission). This cross-correlation function (in general a complex quantity) is the overlap integral between the wave packet at time t and the appropriate final vibrational wave function, acted upon by the transition dipole moment operator

$$C_{\mathrm{if}}(t) = \left\langle \mu\psi_{\mathrm{f}} \right| \exp\left(-\frac{i\hat{H}t}{\hbar}\right) \left| \mu\psi_{\mathrm{i}} \right\rangle \tag{1}$$

where ψ_{i} and ψ_{f} denote the initial and final vibrational wave functions, respectively, in the ground electronic state. Given the cross-correlation function, the Raman scattering cross section for this final state and any excitation frequency can be obtained through a half Fourier transform according to the formula

$$\sigma_{\mathrm{if}}(\omega_{\mathrm{I}}) \propto \omega_{\mathrm{I}}\, \omega_{\mathrm{S}}^3 \left| \int_0^\infty \mathrm{e}^{i(E_{\mathrm{i}} + \hbar\omega_{\mathrm{I}})t/\hbar} C_{\mathrm{if}}(t)\mathrm{d}t \right|^2 \tag{2}$$

(to within a proportionality constant). Here σ stands for the cross section, ω_{I} for the incident electromagnetic frequency, ω_{S} for the scattered frequency, E_{i} for the energy of the initial state (taken to be zero in these calculations), and C_{if} for the appropriate cross-correlation function.

3. Method

The ground and excited-state diabatic potential energy surfaces used for the propagation in this paper are described in Simah et al.[13] To study the effect of the diabatization procedure, we have also applied the scheme of Heumann and Schinke,[5] in which the transition moment between the ground state and the dissociative excited-state becomes zero.

For the purposes of the propagation, it was assumed that the total angular momentum of the excited state is $J = 0$. This is of course not strictly correct, because the photon would excite the initial $J = 0$ state to a $J = 1$ state. In that sense, non-(Born−Oppenheimer) interactions of molecular rotation with electronic degrees of freedom are not taken into account properly. Nevertheless, it is expected that this effect will be small enough not to be important because no rotational structure has been observed in the experimental Raman spectra. Moreover, for the same reason, only the Raman cross sections to the $J = 0$ levels of the ground state (the "Q-branches") are calculated. It is expected that this can give a good overall indication of the relative intensities of the bands.

The ground-state surface for H_2S as calculated by Simah et al.[30] has a minimum at $r(H-S) = 1.3401$ Å (experimental value 1.3366 Å[31]), a bond angle of 92.211° (experimental value 92.226°[31]), and a dissociation energy of 3.78 eV (experimental value 3.9 eV[7]). The ground-state vibrational levels were calculated on this surface using the distributed Gaussian basis approach of Bačić and Light,[32,33] using Radau coordinates[34] to describe the bond distances and angle because of the simple form of the Hamiltonian in these coordinates. "Ray" eigenvectors were calculated at each angle (for which a DVR scheme was used), and through these intermediate eigenfunctions the basis was contracted for the final diagonalization. Eigenfunctions with energies up to 14 300 cm^{-1} above the ground state were used, as this covers essentially the range of the experimental data and also because the Raman lines become rather weak beyond this limit. The convergence of the bound state calculation was verified, and quantum numbers were assigned to states by comparing the energies obtained to those calculated by Halonen and Carrington.[35]

As mentioned above, the initial wave packet is generated simply by multiplying the ground-state wave function by the two transition dipole moment functions for the two excited states. Other than in the diabatization scheme of Heumann and Schinke,[5] in which only the B_1 state was initially populated, in the diabatic representation of Simah et al.[13] the transition dipole moment between the ground and A_2 state is nonzero in C_s symmetry, and therefore both states have an initial population, with about 95% in the B_1 and 5% in the A_2 state. The propagation of the wave packet takes place on a 60×60 Radau coordinate grid, starting at 1.8 bohr with a spacing of 0.07 bohr. The angular grid of the DVR scheme consists of 35 points between 180 and 0 degrees. Because of the large mass of S in relation to the H atoms, the Radau coordinates are very similar to both the more common Jacobi and the internal bond coordinates and can, for visualization purposes, be considered approximately equal to each other.

An expansion of the propagator in terms of Chebyshev polynomials is used for the actual propagation, and the kinetic energy operator is expressed through a fast Fourier transform scheme. The maximum time is 2200 atomic time units (approximately 53 fs, by which time the photodissociation process is essentially complete) and the time step is 4 atomic units. At each point, the value of the cross-correlation function with each of the ground-state levels is calculated and stored. After the propagation is over, each of the correlation functions is half-Fourier transformed to give the "excitation function", i.e., the relative Raman scattering cross section for the appropriate ground-state level. Hence there are two ways of presenting the results. One is as a conventional "Raman stick spectrum" for a particular *excitation frequency* (cross section vs scattered frequency), and the other is the excitation function for a particular *Raman line* (cross section vs excitation frequency). Both ways of presenting the calculated Raman spectra will be used in this paper.

The use of an imaginary optical (absorbing) potential at the ends of the grid is necessary for the propagation in order to avoid unphysical reflection from the grid boundary (which manifests itself as "aliasing" from the back end of the grid because of the FFT propagation scheme). The optical potential suggested by Vibok and Balint−Kurti[36,37] was used, which has the form

$$\epsilon(R) = b \exp\left[-\frac{c}{R - R_0}\right] \tag{3}$$

with parameters $b = 15.0$, $c = 3.5$ bohr, and $R_0 = 4.5$ bohr for both coordinate grids. This is the same as the absorbing potential used by Simah et al. for the calculation of the H_2S absorption spectrum.

4. Results and Discussion

4.1. Ground-State Vibrational Wave Functions. The labeling convention used here for the ground-state levels is in terms of local modes, as also used by Heumann and Schinke.[5] Each vibrational level is labeled with three numbers [*mnk*], where *m* and *n* refer to the number of vibrational quanta in the two H−S oscillators, respectively, and *k* is the number of bending quanta. Because the electric dipole moment operator is symmetric with respect to permutation of the two identical H nuclei, and the initial [000] level is symmetric, any ground-state level to which Raman emission is observed should be symmetric as well. This means that the final states can be represented as as a symmetric linear combination of the local modes

$$|mn^+k\rangle = \frac{1}{\sqrt{2}}(|mnk\rangle + |mnk\rangle) \tag{4}$$

In the following, any reference to the [*mnk*] level will actually imply the [mn^+k] level, unless it is explicitly mentioned otherwise. In Figure 1, some of the ground-state wave functions are shown. Their nodal structure turns out to be very important in understanding the appearance of the spectra. The energies of the most important ground-state levels above the zero point (i.e., the Raman shifts) are listed in Table 1.

4.2. Cross-Correlation Functions. In Figures 2−4, the cross-correlation functions for various final states are shown. The functions in the upper panels were obtained with the potentials and diabatization procedure of Simah et al.,[13] whereas in the lower panels the diabatization method of Heumann and Schinke[5] was applied to the same adiabatic potentials. As can be seen from these figures, a general feature of the absolute values of all cross-correlation functions is an initial increase, followed by a decay to zero. The final decay is obviously due to the eventual advancement of the wave packet (both in coordinate and momentum space) away from the Franck−Condon region. Similarly, the initial low value of the cross-correlation functions can be understood in terms of the initial (at $t = 0$) approximate orthogonality between the wave packet and all ground-state levels. This orthogonality would be exact for all states except

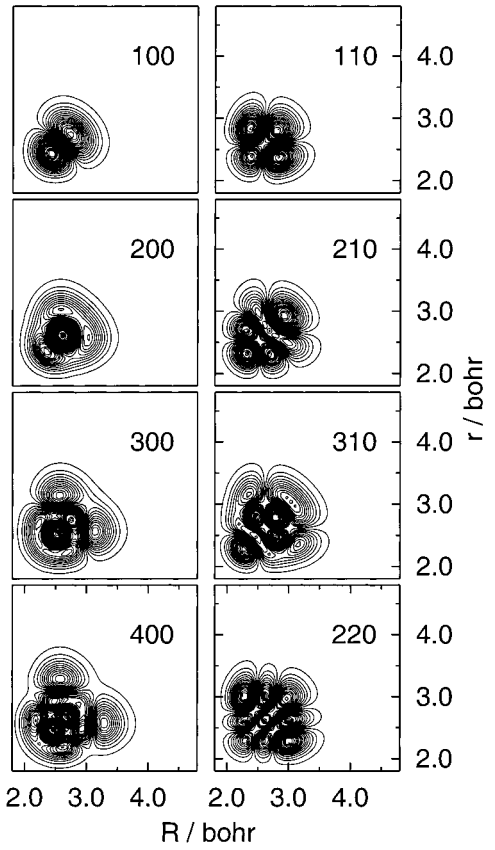

Figure 1. Contour plots of ground-state vibrational wave functions (at the equilibrium bond angle, around 92°). The two axes are the two H−S distances in bohr. The left column comprises the [*n*00] wave functions and it can be seen that their amplitude is very much decreased at high values of the antisymmetric stretch coordinate. This is significantly less the case for the [*n*10] and the [220] wave functions (right column). The contour values range from a minimum of −4.9 to a maximum of +4.9, with a contour distance of 0.2.

TABLE 1: Raman Shifts (in cm^{-1}) of the Most Important Ground State Vibrational Levels (described in the local mode picture)[a]

level description	Raman shift (cm^{-1})	level description	Raman shift (cm^{-1})
001	1185.09	111	6355.73
002	2360.74	202	7391.06
100	2600.28	300	7530.37
003	3526.67	210	7707.17
101	3764.08	301	8648.66
102	4920.70	211	8828.18
200	5116.19	400	9844.25
110	5217.10	310	10124.24
201	6257.29	220	10233.84

[a] The permutation symmetry of the levels is shown in equation 4.

the lowest one if the transition dipole did not depend on the nuclear coordinates.

The cross correlation functions for the [*n*00] lines are typically the largest ones. These functions have no particular further structure apart from some minor recurrences for the highest values of *n*. A qualitative explanation given previously[38,39] for the higher intensity of the [*n*00] lines (outside the region 199−203 nm) is the fact that, as H_2S proceeds down the photodissociation pathway, the vibration is essentially concentrated in *one* H−S bond, and hence the overlap with the corresponding [*n*00] states is higher than that for other [*nm*0] ones. A more "quantum mechanical" insight into this effect is provided if one examines the different structures of the corresponding ground-state wave functions. It is seen from Figure 1 that, as the wave packet bifurcates and its components slide into the exit region, it encounters a much richer nodal structure in the [(*n* − 1)10] rather than the [*n*00] levels, resulting in a lower overlap with the [(*n* − 1)10] states and, hence, a lower absolute value of the cross-correlation function. The same effect has been recognized and commented on by Heumann and Schinke,[5] as well as the fact that the [*n*00] cross-correlation functions decrease with increasing *n* as a result of the richer nodal structure of the higher [*n*00] wave functions. The largest [*n*00] cross-correlation function is the one for [100]. This is presumably due to its lower number of nodes which give it a higher overlap with the evolving wave packet, both at the initial and the final stages of the propagation, despite the larger spatial extent of the higher [*n*00] states.

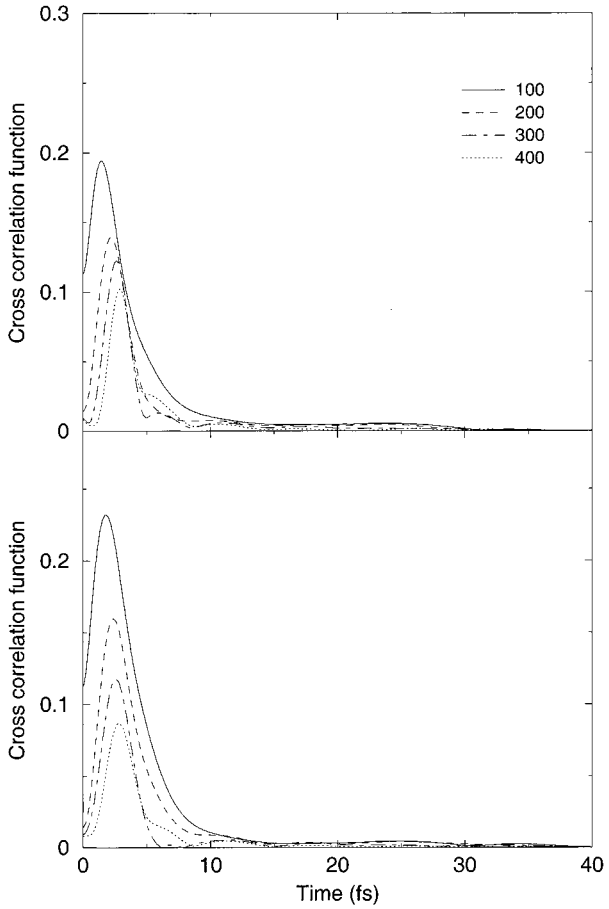

Figure 2. Cross-correlation functions for the main [*n*00] levels. The upper panel refers to the original diabatization of the excited-state surfaces, whereas the lower one refers to the transition dipole moment diabatization (see text).

If one examines the cross-correlation functions of the [*n*10] levels (Figure 3), one sees that the initial decay of the function is much broader due to a recurrence at around 8 fs, which was also observed by Heumann and Schinke.[5] This recurrence is clearly visible in the case of the [110] and [210] levels (as well as the one at 30 fs in the [110] case). It cannot be clearly seen in the [310] case, but even there the cross-correlation function has a shoulder at about 8 fs. Heumann and Schinke[5] have observed that, if the coupling between the two surfaces is switched off, this recurrence disappears. We have confirmed the same effect by propagating the wave packet independently on the two surfaces with zero coupling. The pattern of initial build up followed by a decay persists, although now the magnitude of the cross-correlation functions is much larger and

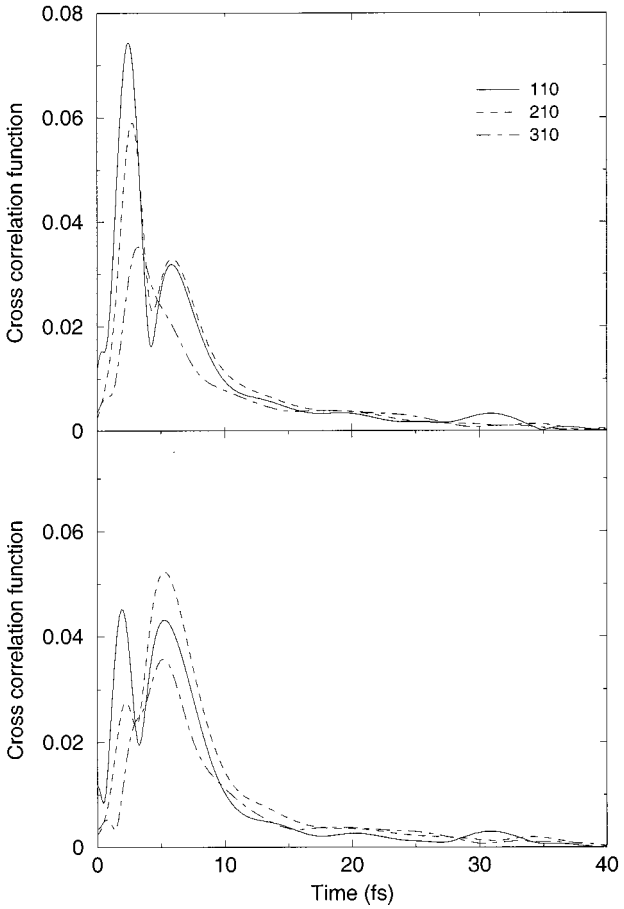

Figure 3. Cross-correlation functions for the main [*n*10] levels.

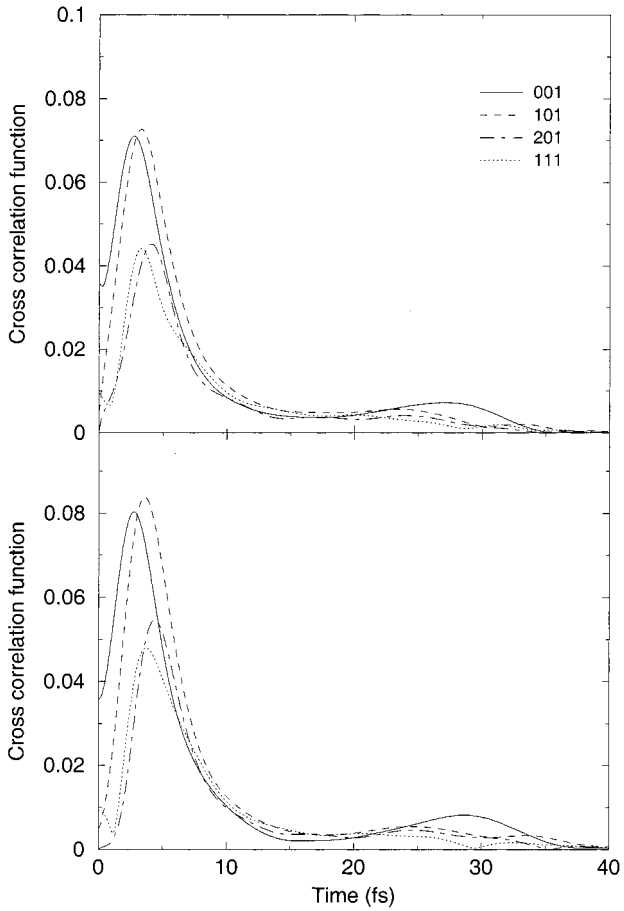

Figure 4. Cross-correlation functions for the main [*mn*1] levels.

no short-time recurrence is seen any more. Clearly, therefore, the recurrence is a consequence of the inter-surface coupling. The same conclusion was reached by Heumann and Schinke,[5] but they were not able to find an explanation for this effect.

We have carefully examined the evolving wave packet in order to unravel the effect causing the recurrence. Looking at the evolving wave packet in Figures 5 and 6, we see that its bound state component (Figure 5) develops "wings" in a short time (around 3 fs). These are a consequence of the coupling between the bound and the dissociative surfaces. This coupling increases with increasing distance from the C_{2v} line. As is seen from the figures, the wave packet starts moving down the dissociation pathway (Figure 6), but the coupling brings part of this back into the bound surface. As a result of this, also the original wave packet has these components (wings) attached to it after a short interval. The increase in the cross-correlation function leading to the recurrence occurs at a time of about 5−6 fs. It can be seen that, at this time, the lateral components of the wave packet (on both surfaces) have centers around 3.8 bohr and are moving outward, away from the range of the ground-state wave functions. Examining these wave functions (Figure 1), one sees that the [(n − 1)10] ones have a much higher amplitude *away* from the C_{2v} line than do the [n00] ones. Moreover, this is of the *opposite* sign to the amplitude on the C_{2v} line. This implies that the initial wave packet would have negative overlap with these states in this part of coordinate space (relative to the overlap near the C_{2v} line). Thus, a possible explanation of the recurrence is the advancement in momentum space (and the consequent "dephasing") of the wings as they move down the dissociation coordinate (on both the bound and the dissociative surfaces), and the consequent reduction of negative overlap with the [110] and [210] states. Another factor contributing to this would be the (small) difference in energy between the two surfaces, which has the consequence of "rotating" the phase of the wings relative to the central component, once again reducing the negative overlap. The effect would be much less pronounced in the [310] state because, as it can be seen in Figure 1, its nodal structure is much richer in the wing region and the initial negative overlap is very small to begin with. It is important to stress, though, that apart from the phase of the lateral components there is an interplay of various factors here (such as the timing of the central wave packet component overlapping with the "positive" lobe of the [110] and [210] functions and *its* de-phasing), and it is not at all easy to reach definite conclusions. Another important point is that the previous qualitative arguments make an implicit Franck−Condon assumption, i.e., that the magnitude of the transition dipole moment does not vary much with the nuclear coordinates in the regions where both the ground-state wave functions and the evolving wave packet have significant amplitude (strictly, the overlap of the wave packet with the dipole-multiplied wave functions should be considered). We have found this assumption to be good enough to justify the previous arguments by inspection of the transition dipole moments.[30]

When the alternative diabatization method of Heumann and Schinke is used, according to which the transition dipole moment to one of the surfaces becomes zero, some differences can be seen in the cross-correlation functions. Specifically, in the case of the [n00] levels (Figure 2), the maximum of the cross-correlation function is higher for the alternative method. We believe this to be an effect of the weaker coupling potential between the two surfaces, which does not diminish as effectively the wave packet amplitude on the bound surface, resulting in

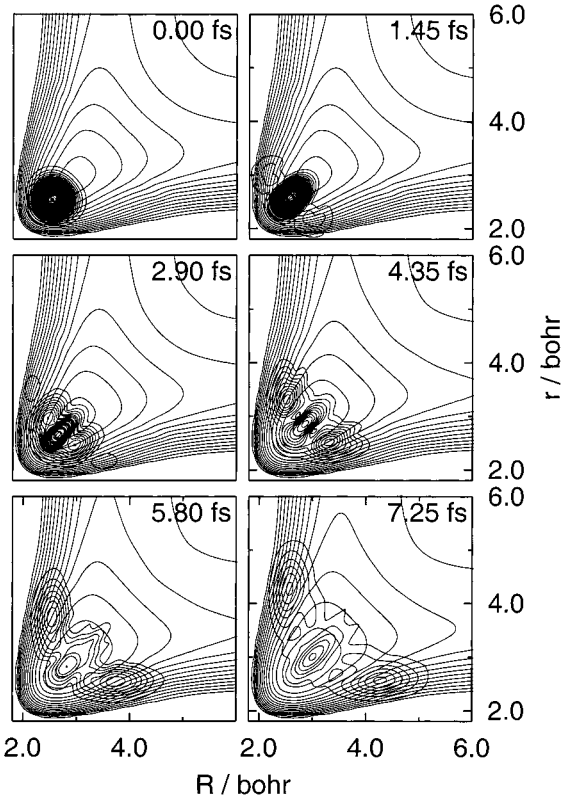

Figure 5. Modulus of the wave packet component on the bound surface at various times (at the angle of maximum population). The two axes are the two H−S distances in bohr. The value of the minimum contour for the bound potential surface is 0.21 hartree (except at 7.25 fs, where it is 0.22 hartree at this angle) and the contour distance is 0.01 hartree. The maximum contour value for the wave packet is 5.0, the contour distance is 0.04.

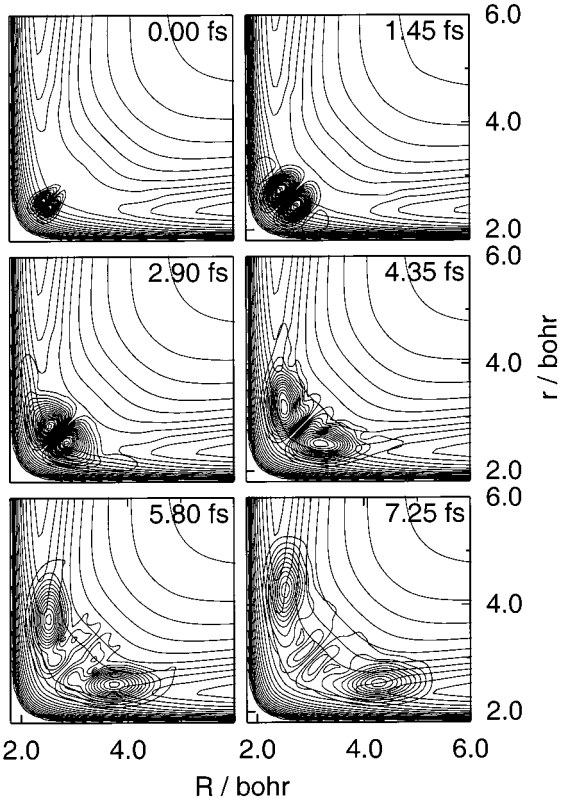

Figure 6. Same as Figure 5 for the dissociative surface (with the same wave packet contour spacings). The amplitude on the C_{2v} line is always zero, because both the transition dipole from the ground surface and the coupling with the excited bound surface are zero on this line by symmetry. The minimum contour for this surface (the farthest one in the exit channels) is at 0.17 hartree, with a contour distance of 0.01 hartree.

higher overlap with the bound state levels. Interestingly, in the case of the [*n*10] levels (Figure 3), the initial maximum is appreciably *lower* for the alternative diabatization method. The origin of this effect is more subtle, and we attribute this to the fact that, because of the weaker intersurface coupling, the *lateral* components of the wave packet (away from the C_{2v} line) are not diminished in amplitude and contribute *negatively* to the cross-correlation function through overlap with the negative lobes of the wave functions at high values of the antisymmetric stretch coordinate (this is most easily seen on the structure of the [110] wave function, considering the relative signs of the lobes).

A further effect which is seen in the cross-correlation functions relating to levels with one quantum of bending excitation ([*mn*1], Figure 4) is a recurrence around 25−30 fs, which can also be seen in the [110] correlation function but is almost invisible in the [*n*00] ones. Otherwise, the cross-correlation functions for [*mn*1] states are generally of intermediate width (broader than those for the [*n*00] states). As is seen in Figure 7, the angle with maximum population in the bound surface goes through a minimum (∼85°) at about 15 fs and recurs at about 30 fs. It is presumed that this recurrence is what is seen at the excited bending levels. The fact that it is more pronounced for the levels with one bending quantum can probably be attributed to the sharper "bending-excited" wave function (with one angular node) that makes the recurrence "steeper". Also, a recurrence of the wave packet with roughly the same period (30 fs) has been attributed[4,13] to the symmetric stretch motion in the bound state, and it certainly would be expected to contribute to these recurrences as well.

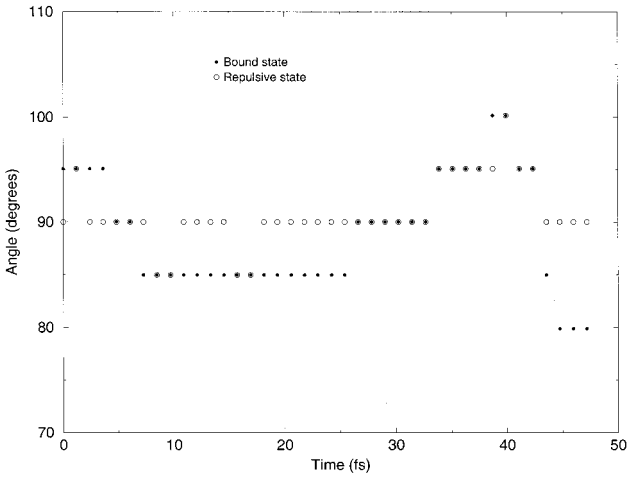

Figure 7. H−S−H angles of maximum population for the two excited-state surfaces, as a function of time. The angles are chosen from the range of the DVR angles used to represent the function, leading to the discrete nature of the graph.

Finally, with the alternative diabatization method, no appreciable difference is seen in the shape of the [*mn*1] cross-correlation functions apart from their increased magnitude, in a similar way to the [*n*00] functions.

4.3. Excitation Functions. In Figures 8−10, the excitation functions corresponding to the cross-correlation functions in Figures 2−4 are shown. Again, the upper and lower panels refer to the diabatization methods of Simah et al.[13] and Heumann and Schinke,[5] respectively. To an excellent approximation, the

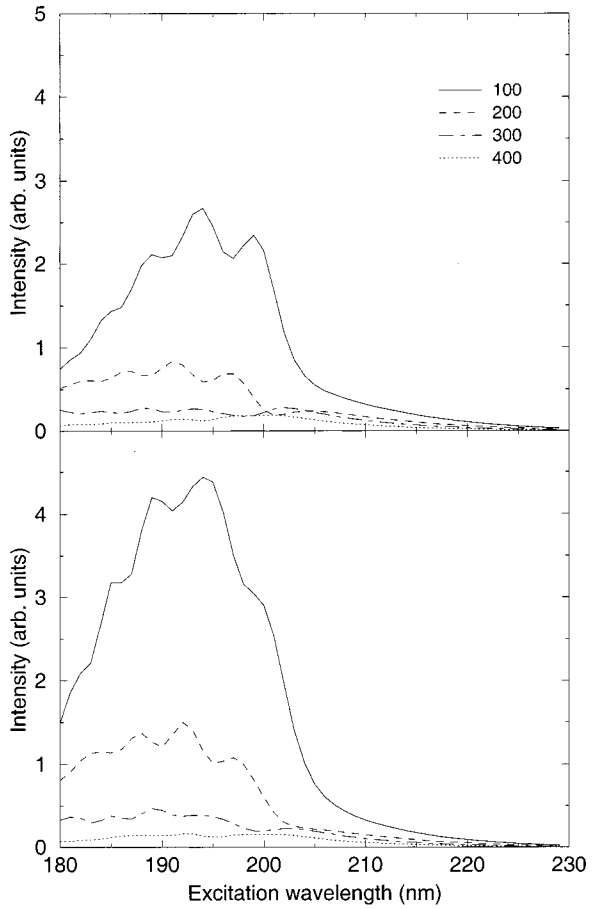

Figure 8. Excitation functions for [*n*00] levels. The upper panel refers to the original diabatization of the excited-state surfaces, whereas the lower one refers to the transition dipole moment diabatization (see text).

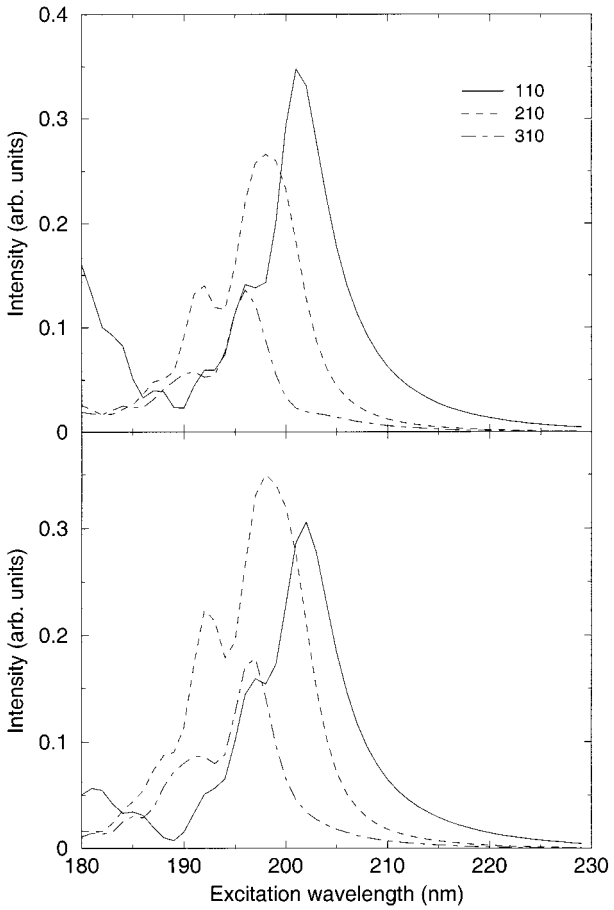

Figure 9. Excitation functions for[*n*10] levels.

phases (i.e., the arguments) of the cross-correlation functions are linear functions of time and, hence, the bandwidth theorem of Fourier transforms can be safely applied. Therefore, the narrowness of the [*n*00] cross-correlation functions should lead to a broad dependence of the corresponding cross sections on the excitation wavelength, which is indeed borne out by the excitation functions in Figures 8−10. The largest among them is the [100] excitation function, in accordance with the fact that it has the highest cross-correlation function.

From the recurrences in the cross-correlation functions for the [*mn*1] final states discussed above, the excitation functions for [*mn*1] states would be expected to show a narrower overall width than the corresponding [*n*00] ones with pronounced periodic peaks on top. This is exactly the picture seen in the excitation functions for these [*mn*1] levels in Figure 10, with the peaks being presumably due to both the angular as well as the symmetric stretch recurrences. An additional feature which corroborates this is the fact that the *spacing* of the peaks in the excitation function is similar to the one observed in the absorption spectrum of H_2S, which has been attributed to the symmetric stretch recurrence at exactly this time (25−30 fs).[4,13]

The final features to be explained are the excitation functions pertaining to the ground state [*n*10] levels. In sharp contrast to the [*n*00] functions, these appear to be rather narrow and concentrated in the region around 195−200 nm. Moreover, some periodic structure can be seen in them, although it is by no means as clear-cut as that of the previously mentioned [*mn*1] functions. Browning et al.[39] attribute the sudden acquisition of intensity of [*n*10] lines around 200 nm to the fact that this energy region closely probes the conical intersection of the two surfaces. As a result of this, there is considerable crossing over to the dissociative surface for these excitation wavelengths and hence considerable action in the antisymmetric stretch coordinate, which leads to increased Raman emission to [*n*10] levels. The form of the excitation function can be easily understood in terms of the shape of the corresponding cross-correlation function. The aforementioned short-time recurrence for [*n*10] levels has the effect of increasing the overall width of this function in time. This broadness, in conjunction with the linearity of its phase with time, leads to a narrow shape of the excitation functions as well as periodic structure with large spacing. The latter is seen at the low wavelength end of the excitation functions, where the intensity of the [110] line is seen to rise again. It would be interesting to perform Raman scattering experiments at this low wavelength region to verify this effect of the [*n*10] lines regaining intensity. The periodic structure with small spacing in the excitation functions can, as in the case of the [*mn*1] lines, be attributed to the long-time recurrence in the cross-correlation function (presumably due to the symmetric stretch motion).

Considering the effects of the alternative diabatization method on the excitation functions, it can be seen that they increase the intensity of the spectra in the [*n*00] and [*mn*1] cases, without any other appreciable qualitative change. This is of course to be expected, on account of the larger magnitudes of the cross-correlation functions, mentioned earlier. In the [*n*10] case, one can see a dramatic increase in the intensity of the [210] line relative to the [110] one. This can easily be seen to be due to the fact that the short-time recurrence peak for the [210] cross-correlation function is larger than the corresponding one for [110].

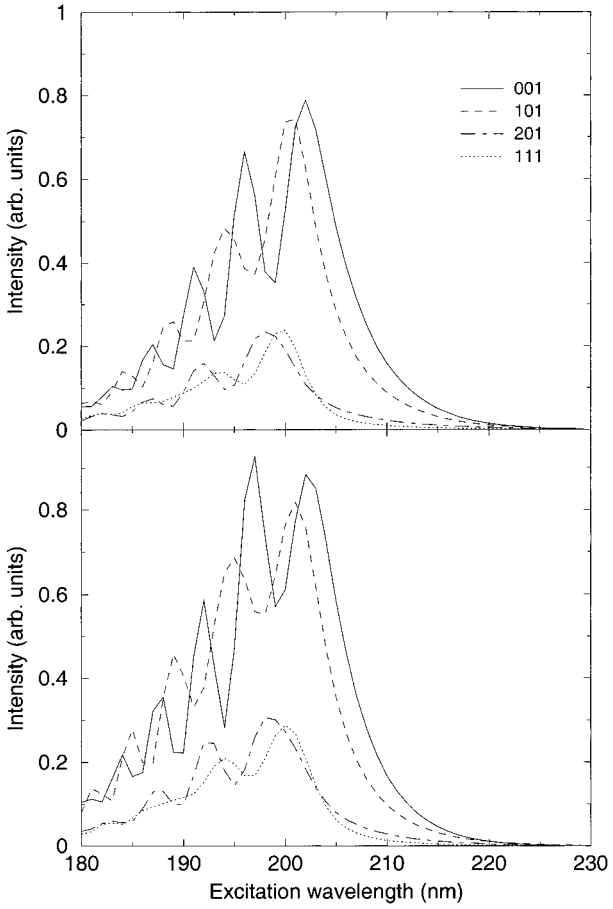

Figure 10. Excitation functions for[*mn*1] levels.

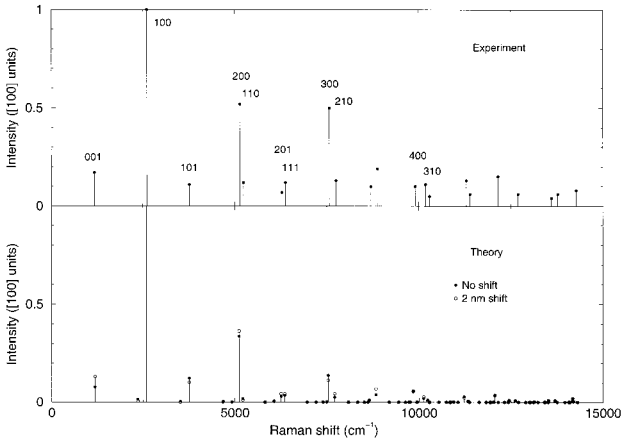

Figure 11. Calculated and experimental H_2S Raman spectra for an excitation wavelength of 188 nm. The units in both the experimental and the theoretical spectra are those of the [100] line in the current spectrum. Filled circles in the theoretical spectra correspond to the original surfaces, whereas open ones correspond to excitation functions shifted by 2 nm to lower wavelengths.

4.4. Comparison with Experiment. The spectra presented in Figures 11−14 are the analogous ones that were published by Heumann and Schinke[5] (i.e., with excitation wavelengths 188, 192, and 204 nm). In addition, the spectrum at 200 nm is given. The spectra shown are those obtained with the diabatization method of Simah et al.,[13] as these results were generally in better agreement with experiment than were those with the transition dipole diabatization (although the differences were minor). The most recent experimental data on the H_2S Raman emission spectra whose intensities are cited are those of

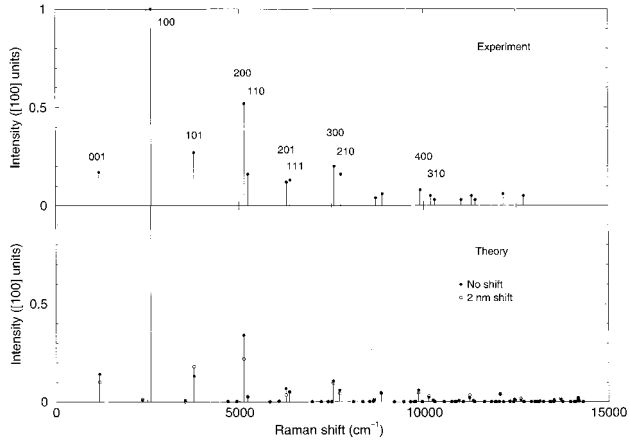

Figure 12. Same as Figure 11 for an excitation wavelength of 192 nm.

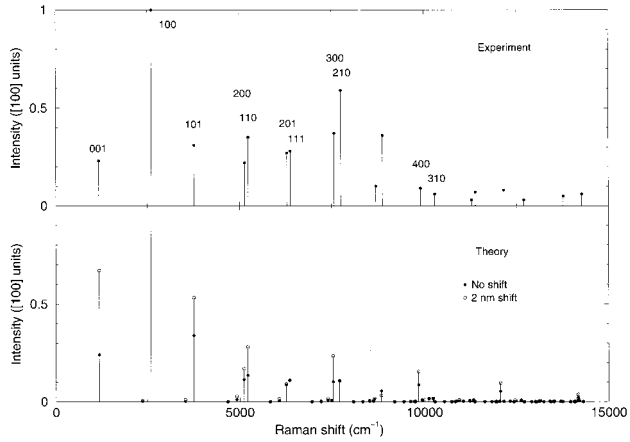

Figure 13. Same as Figure 11 for an excitation wavelength of 200 nm.

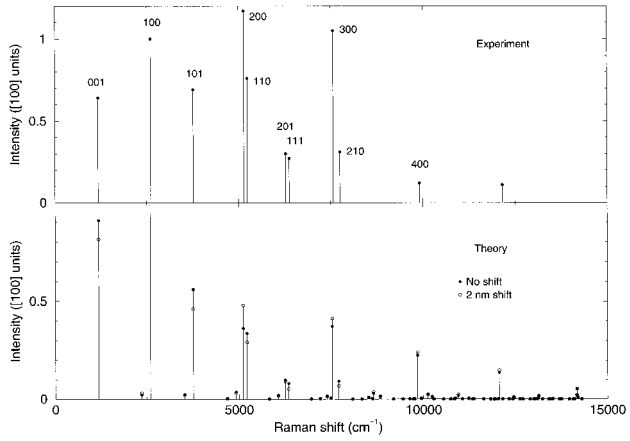

Figure 14. Same as Figure 11 for an excitation wavelength of 204 nm.

Brudzynski et al.[24] In this spectrum, absolute line intensities cannot be immediately compared for different excitation wavelengths as, in all cases, the cross sections have been normalized with respect to the [100] line for the particular excitation wavelength. The unfortunate fact is that the excitation function of the [100] emission varies rapidly across 200 nm (cf. Figure 8), which makes comparison even more prone to errors, since small discrepancies in the computed excitation energy can cause large ones in the relative intensities. To demonstrate this effect, two theoretical Raman spectra are shown in each case. One uses the original surfaces (filled circles), while the other (open circles)

shifts all excitation functions to lower wavelengths by 2 nm. A similar energy shift was needed to reproduce the experimental line positions in the simulation of the absorption spectrum.[13] It can be seen that, especially in the 200 nm region, the effect of the shift is quite appreciable.

As a rule, the [*n*00] lines are the strongest ones throughout the excitation wavelength range. This is an effect of the higher values of the corresponding cross-correlation functions in conjunction with Parseval's theorem for Fourier transforms, which states that the total intensity of a function is preserved in a Fourier transformation. This is clearly seen in both the 188 nm and the 192 nm cases. In this region of excitation wavelengths, the [(*n*-1)10] lines are, as seen in both theory and experiment, weaker than their [*n*00] counterparts on account of their narrow excitation functions. Especially at 188 nm, it is obvious that the [200] line is more than three times more intense than the [110] one in the experiment (even more so in theory); similar ratios are found for the [300]/[210] and [400]/[310] pairs. The picture is not much different at 192 nm, although now it can be seen that the [*n*10] lines are rapidly picking up intensity. In the experiment, the [200] line is now roughly 2.5 times more intense than [110] (in the theory it is still a lot stronger), but now the [300] and [210] lines are of comparable intensity in both theory and experiment.

It can be seen from the excitation functions that this should be an area of considerable variation of the intensities of lines with bending excitation (owing to the periodicity caused by the recurrence). At 188 nm, the experimental intensities of the [001] and [101] lines are similar to these of the [*n*10] lines, whereas the corresponding theoretical ones are about twice higher. This is still the case at 192 nm. However, it should be borne in mind that these intensities could change rapidly with a small change of the recurrence features (because of the high excitation energy dependence).

In the region around 200−204 nm (the region of the conical intersection), the normalizing line ([100]) falls rapidly in intensity, and even a small shift of its excitation function can change the relative intensities dramatically, as demonstrated in Figure 13. As a result, we do not think that a comparison of intensities *across* the excitation wavelengths would be very fruitful, although useful conclusions can still be drawn from comparing lines within the same Raman spectrum. The spectrum with an excitation wavelength of 200 nm is almost exactly the region where the excitation functions of the [110] and [210] lines reach a maximum. It is the only excitation wavelength in the experimental and the theoretical spectra where the [110] line is stronger than the [200], and, in the case where the surfaces are unshifted, the [210] line is also stronger than the [300] (this is an area of very steep variation of the intensity of the [210] line, as seen from its excitation function). As mentioned before, this is due to the peculiarly narrow excitation function for these lines arising from the broad cross-correlation functions. At this point it should be stressed that the dipole moment diabatization scheme predicts a much narrower region of [110]/[200] intensity inversion, which does not include 200 nm, and hence does not predict this effect (although the [210]/[300] intensity inversion is predicted). The lines with one quantum in the bending mode ([001] and [101]) also pick up intensity in this region (as seen in the corresponding excitation functions) and, in both the theoretical and experimental spectra, have an intensity roughly four times lower than the [100] line in the case of the unshifted surfaces. The shifted surfaces give much higher intensities for these lines, which is not unexpected seeing the sharp variation of the excitation functions. The relative intensity (wrt [100]) of the [110], [200], [111], and [201] lines are not that well reproduced; they appear to be much stronger in the experimental spectrum ([110] is roughly half the intensity of [100] compared to roughly one-sixth in the theoretical spectrum). But because this is a region where both the [100] line and the [*n*10] lines are expected to vary much in intensity (as mentioned previously), such comparisons are exceedingly open to error. Thus, in the case where the surfaces are shifted, the intensities of [200] and [110] are considerably more in agreement with experiment. The Raman spectrum of H_2S with an excitation wavelength of 200 nm is also within the region covered by Browning et al.,[39] and our theoretical spectra appear to be in good qualitative agreement with it (although no intensities are given in the paper). Furthermore, there appears to be at least one point of qualitative disagreement between the Browning and Brudzynski results: this concerns the intensity of the [210] line (at 200 nm) in relation to the [100] line. The [210] line is about 0.59 times the intensity of the [100] one in the Brudzynski results, whereas it appears that this ratio is appreciably lower in the Browning results.

In the 204 nm region, the [100] line is expected to have dropped to about a third of its original intensity from its excitation function. This is reflected in the experimental spectrum by the fact that almost all lines show a dramatic *increase* in intensity, which is almost certainly attributable to the diminution of the normalizing line. This is true for both the [*n*00] lines and the lines with bending excitation [001] and [101], which while absolutely dropping in intensity (in the theoretical spectrum) they are rising in relation to [100]. Exceptions to this are the [201], [111], and [210] lines, which are also expected to fall off in intensity at this excitation wavelength. Here the [*n*00] lines are again stronger than their [(n − 1)10] counterparts (as we are off the [*n*10] peak), and once more they dominate the spectrum. A rather dramatic effect though is the fact that both the [200] and the [300] lines are *stronger* than the [100] line, something that is definitely not seen in the theoretical spectra (both lines have about half the intensity of [100]) and it is also not suggested by the nearby (203 nm) Raman spectrum taken by Browning. It is highly probable that the rapid variation of the [100] line in this region leads to an error of underestimation of the intensities of the [*n*00] lines. Finally, it should be mentioned that in all cases (except perhaps for 204 nm) many theoretical lines with very high Raman shifts (above 10 000 cm^{-1}) are very much weaker than the corresponding experimental shifts (and hence the cube of the scattered frequency appearing in the intensity expression cannot by itself account for their relative weakness). Of course, lower relative magnitudes of the cross-correlation functions are to be expected because of the richer nodal structure of the corresponding ground state wave functions, and it is probably the case that significant changes in these magnitudes can be achieved with some fine-tuning of the potential energy surfaces and couplings.

5. Conclusion

The Raman emission spectrum of photodissociating H_2S in the region of its first absorption band has been calculated using time-dependent wave packet propagation on a surface by Simah et al.[13] Two alternative diabatization methods have been used for the surfaces, the original one by Simah et al. and one based on the transition dipole moments, used by Heumann et al.[5] In the majority of cases, the former one has been found to give results in closer agreement with experiment, although the differences are generally minor. Excitation functions have been calculated for several Raman lines spanning the range of the

absorption spectrum of H_2S, and their various features have been interpreted in terms of the corresponding cross-correlation functions. In particular, it has been shown that, with the surface used, the excitation functions of [*n*00] levels (where all energy is localized in one oscillator) should not show a very strong dependence on the excitation wavelength (apart from the [100] level), whereas those of [*n*10] levels should have a narrow peak around 200 nm. This peak can be attributed (in a time-independent framework) to the excitation in the vicinity of the conical intersection (as noted by Browning et al.[39]) or (in a time-dependent framework) to the broadness of the cross-correlation functions arising from the intersurface coupling. Moreover, the levels with one quantum of bending motion show excitation functions with strong periodicity (less so in the case of the [*n*10] functions), and this has been attributed to a long time recurrence in the cross-correlation function arising from both the bending and the symmetric stretch motions.

The calculated spectra have been compared to those obtained by Brudzynski et al.[24] Although several of the experimental features are reproduced by the calculations, there are still serious discrepancies remaining. A difficulty to be removed is the fact that the experimental Raman lines are normalized with respect to the [100] line for each excitation wavelength, which makes comparison troublesome, especially in regions where the intensity of this line varies rapidly. More accurate experimental data will be indispensable for the further elucidation of the H_2S Raman emission spectrum.

Acknowledgment. This work was funded by the Deutsche Forschungsgemeinschaft as part of the Schwerpunktprogramm "Zeitabhängige Phänomene und Methoden in Quantensystemen der Physik und Chemie". The authors acknowledge David Simah for his contribution in the calculation of the H_2S potential energy surfaces.

References and Notes

(1) Lee, L. C.; Wang, X.; Suto, M. *J. Chem. Phys.* **1987**, *86*, 4353.
(2) Heumann, B.; Düren, R.; Schinke, R. *Chem. Phys. Lett.* **1991**, *180*, 583.
(3) Schinke, R.; Weide, K.; Heumann, B.; Engel, V. *Faraday Discuss. Chem. Soc.* **1991**, *91*, 31.
(4) Heumann, B.; Weide, K.; Düren, R.; Schinke, R. *J. Chem. Phys.* **1993**, *98*, 5508.
(5) Heumann, B.; Schinke, R. *J. Chem. Phys.* **1994**, *101*, 7488.
(6) van Veen, G. N. A.; Mohamed, K. A.; Baller, T.; de Vries, A. E. *Chem. Phys.* **1983**, *74*, 261.
(7) Xie, X.; Schnieder, L.; Wallmeier, H.; Boettner, R.; Welge, K. H.; Ashfold, M. N. R. *J. Chem. Phys.* **1990**, *92*, 1608.
(8) Continetti, R. E.; Balko, B. A.; Lee, Y. T. *Chem. Phys. Lett.* **1991**, *182*, 400.
(9) Hawkins, W. G.; Houston, P. L. *J. Chem. Phys.* **1980**, *73*, 297.
(10) Hawkins, W. G.; Houston, P. L. *J. Chem. Phys.* **1982**, *76*, 729.
(11) Ashfold, M. N. R.; Schnieder, L.; Welge, K. H. *Faraday Discuss. Chem. Soc.* **1991**, *91*, 128.
(12) Dixon, R. N.; Marston, C. C.; Balint-Kurti, G. G. *J. Chem. Phys.* **1990**, *93*, 6520.
(13) Simah, D.; Hartke, B.; Werner, H.-J. *J. Chem. Phys.* **1999**, *111*, 4523.
(14) Lee, S.-Y.; Heller, E. J. *J. Chem. Phys.* **1979**, *71*, 4777.
(15) Hartke, B. *Chem. Phys. Lett.* **1989**, *160*, 538.
(16) Butler, L. J. *Chem. Phys. Lett.* **1991**, *182*, 393.
(17) Kleinermanns, K.; Linnebach, E.; Suntz, R. *J. Phys. Chem.* **1987**, *91*, 5543.
(18) Shih, S.; Peyerimhoff, S. D.; Buenker, R. J. *Chem. Phys.* **1976**, *17*, 391.
(19) Weide, K.; Staemmler, V.; Schinke, R. *J. Chem. Phys.* **1990**, *93*, 861.
(20) Theodorakopoulos, G.; Petsalakis, I. D. *Chem. Phys. Lett.* **1991**, *178*, 475.
(21) Thompson, S. D.; Carroll, D. G.; Watson, F.; O'Donnell, M.; McGlynn, S. P. *J. Chem. Phys.* **1966**, *45*, 1367.
(22) Andresen, P.; Schinke, R. In *Molecular Photodissociation Dynamics;* Ashfold, M. N. R., Baggott, J. E., Eds.; The Royal Society of Chemistry: London, 1987.
(23) Engel, V.; Staemmler, V.; Vander Wal, R. L.; Crim, F. F.; Sension, R. J.; Hudson, B.; Andresen, P.; Hennig, S.; Weide, K.; Schinke, R. *J. Phys. Chem.* **1992**, *96*, 3201.
(24) Brudzynski, R. J.; Sension, R. J.; Hudson, B. *Chem. Phys. Lett.* **1990**, *165*, 487.
(25) Loudon, R. *The Quantum Theory of Light*; Oxford University Press: Oxford, 1994.
(26) Schinke, R. *Photodissociation Dynamics*; Cambridge University Press: Cambridge, 1993.
(27) Hartke, B. *J. Raman Spectrosc.* **1991**, **22**, 131.
(28) Kramers, H. A.; Heisenberg, W. *Z. Phys.* **1925**, *31*, 681.
(29) Dirac, P. A. M. *Proc. R. Soc. London* **1927**, *114*, 710.
(30) Simah, D. These de Doctorat; Université De Marne-la-Vallée: France, 1999.
(31) Kozin, I. N.; Jensen, P. *J. Mol. Spectrosc.* **1994**, *163*, 483.
(32) Bačić, Z.; Light, J. C. *J. Chem. Phys.* **1986**, *85*, 4594.
(33) Bačić, Z.; Light, J. C. *J. Chem. Phys.* **1987**, *86*, 3065.
(34) Bačić, Z.; Watt, D.; Light, J. C. *J. Chem. Phys.* **1988**, 89, 947.
(35) Halonen, L.; Carrington, T., Jr. *J. Chem. Phys.* **1987**, *88*, 4171.
(36) Vibók, A.; Balint-Kurti, G. G. *J. Chem. Phys.* **1992**, *96*, 7615.
(37) Vibók, A.; Balint-Kurti, G. G. *J. Phys. Chem.*, **1988**, *92*, 2087.
(38) Person, M. D.; Lao, K. Q.; Eckholm, B. J.; Butler, L. J. *J. Chem. Phys.* **1989**, *91*, 812.
(39) Browning, P. W.; Jensen, E.; Waschewsky, G. C. G.; Tate, M. R.; Butler, L. J.; Hessler, J. P. *J. Chem. Phys.* **1994**, *101*, 5652.